New routes for production of proton-rich Tc isotopes

Moumita Maiti* and Susanta Lahiri†
Chemical Sciences Division, Saha Institute of Nuclear Physics, 1/AF, Bidhannagar, Kolkata 700 064, India
(Received 15 August 2009; published 10 February 2010)

Proton-rich Tc radionuclides have been identified as potential candidates for specific clinical and biological applications in the last decade. So far, these radionuclides have been produced either by proton-induced reaction on Mo targets or α-particle-induced reaction on Nb targets. This article lightens two heavy-ion-induced production routes of ^{93,94,95,96}Tc radionuclides through ^{7}Li + ^{nat}Zr and ^{9}Be + ^{nat}Y reactions and provides important cross-sectional information in the projectile energy ranges 37–45 MeV and 30–48 MeV, respectively. Excitation functions of those reactions have been measured using the stacked-foil technique followed by the off-line γ-spectrometric studies. Measured cross-sectional data have been interpreted comparing theoretical predictions of the two nuclear reaction model codes PACE-II and ALICE91. Experimental cross sections agreed with the theory. Measured production cross sections of ^{94,95}Tc have been compared with those produced from the α + ^{93}Nb reaction.

DOI: 10.1103/PhysRevC.81.024603 PACS number(s): 24.60.Dr, 25.70.Gh

I. INTRODUCTION

Tc has been an element of interest over the last three decades because of its several elegant features and practical applications, particularly in the field of nuclear medicine. Out of the identified Tc isotopes, 21 are proton-rich, having a β^+ and/or ϵ decay mode, while the remaining 20 are neutron-rich and mostly β^- emitters. Neutron-rich Tc isotopes are mostly short-lived, except ^{98}Tc ($T_{1/2}$ = 4.2 Myr) and ^{99}Tc ($T_{1/2} = 2.111 \times 10^5$ years). The only radioisomer, ^{99}Tc^m, is extensively used in nuclear medicine because of its half-life ($T_{1/2}$ = 6.01 hours) and 140.474 keV γ ray, both of which are suitable for *in vivo* imaging. In fact, every year, millions of people are diagnosed using ^{99}Tc^m around the globe. However, neutron-rich Tc radionuclides, even ^{99}Tc^m, are not well suited because of extremities in terms of half-lives for laboratory experiments of tens of hours in duration. On the other hand, proton-rich γ- and β^+-emitting Tc tracers (^{93}Tc, ^{94}Tc^m, ^{94}Tc, ^{95}Tc^m, ^{95}Tc, ^{96}Tc) exhibit salient features for serving diverse applications, especially for studying long metabolic processes. For example, ^{94}Tc^m ($T_{1/2}$ = 52.0 min, I_{β^+} = 70.2%, E_{β^+} = 2.44 MeV) is a potentially promising radionuclide for the positron emission tomography of organs. Short-lived γ emitters ^{93}Tc ($T_{1/2}$ = 2.75 hours) and ^{94}Tc ($T_{1/2}$ = 293 min) are convenient for short-span experiments, whereas ^{95}Tc, which has a comparatively long half-life of 20 hours, can be useful in keeping track of the metabolic function of the human brain and heart. Therefore information on the nuclear data for the production of proton-rich Tc tracers having considerable half-life is important.

Usually, proton-rich Tc tracers are produced in the medium-energy accelerators using light-ion-induced (p, d, ^{3}He, α) reactions on molybdenum (Mo) or niobium (Nb) targets. To investigate nuclear reactions and structure, Tc isotopes are produced by α- and ^{3}He-induced reactions on mononuclidic ^{93}Nb targets [1–7]. A large number of reports are available on the excitation functions of Tc radionuclides from proton- and deuteron-induced reactions on natural Mo as well as enriched Mo isotopes covering a wide energy range [5,8–15]. Moreover, cross sections of ^{95,96}Tc and ^{96}Tc^m have also been measured by neutron-induced reactions on enriched ^{96}Ru as well as natural Ru targets [16,17]. Even production of ^{95,96}Tc by proton- and γ-ray-induced reactions on ^{99}Tc have been reported in Ref. [18].

However, cross-sectional data of the proton-rich Tc isotopes produced via heavy-ion-induced reactions are rare. A few articles are available where excitation functions are measured from ^{12}C-induced reactions on natural niobium (^{93}Nb) and natural yttrium (^{89}Y) [19,20] with the aim of studying the reaction mechanisms involved in the particular reaction. Unlike the neutron- and light-charged particle reactions, understanding of reaction mechanisms and the cross-sectional data of heavy ion reactions is not adequate to date and hence demands attention.

To satisfy the growing demand of nuclear data of clinically and biologically important proton-rich Tc isotopes, in this article, we have investigated two separate production routes. Excitation functions of evaporation residues produced in ^{7}Li + ^{nat}Zr and ^{9}Be + ^{nat}Y reactions have been measured in the incident energy ranges 37–45 MeV and 30–48 MeV, respectively, using a stacked-foil technique followed by off-line γ-spectrometric studies. Experimental measurement of the formation cross sections of the desired radionuclides and the associated impurities is mandatory to propose a new production route for clinical radionuclides. The word *impurity* from the perspective of nuclear medicine has been defined in our recent article [21]. The impurity describes all other evaporation residues (stable as well as radionuclidic) and their decay products, including the decay of compound nuclei, except the particular radionuclide of interest. Quantification as well as reduction of those impurities by selecting proper nuclear reaction parameters, such as incident energy and target thickness, are important. The cross-sectional data provide an idea of selecting those parameters. Enriched isotopes can reduce the production of impurities but are quite expensive.

*moumita.maiti@saha.ac.in
†susanta.lahiri@saha.ac.in

Naturally occurring mononuclidic elements are therefore preferred as target material to prevent the opening of fewer reaction channels. However, it is also possible to use stable elements with more than one naturally occurring isotope, provided that the production parameters are controlled.

In this article, our goal is therefore twofold:

(i) Measurement of the excitation functions of ^{7}Li + ^{nat}Zr and ^{9}Be + ^{nat}Y reactions
(ii) Investigation of the reaction mechanisms involved in those two reactions.

Broadly, nuclear reaction is understood in terms of three reaction mechanisms, namely, direct (DIR), preequilibrium (PEQ), and equilibrium or evaporation (EQ). The cross section of the product nuclei corresponding to a particular reaction is the result of all the reaction mechanisms involved. In this article, contributions from DIR reaction processes are not expected because of low incident energies. We have tried to explain the experimental cross sections of the evaporation residues in terms of PEQ and EQ reactions in the incident energy ranges 37–45 MeV and 30–48 MeV, respectively, as the existence of PEQ emission has also been observed in some cases in such low energies using nuclear reaction model codes PACE-II [22] and ALICE91 [23,24].

The experimental procedure is described in Sec. II. Section III presents discussions about the brief formalisms followed in the codes PACE-II and ALICE91 for the theoretical calculation, and Sec. IV deals with the results and discussion of the present work.

II. EXPERIMENTAL PROCEDURE

A. Irradiation parameters

1. ^{7}Li + ^{nat}Zr

Pure metallic Zr foil (99.94%) was procured from Johnson Matthey. Self-supporting metallic Zr foils of 3 mg/cm^2 thickness were prepared by proper rolling. Experiments were carried out at the Bhabha Atomic Research Centre (BARC)-Tata Institute of Fundamental Research (TIFR) Pelletron at Mumbai, India. The stack of the target-catcher assembly was prepared by placing a Zr foil followed by aluminum catcher foils, procured from E-Merck, Germany, of thickness 1.5 mg/cm^2 and was bombarded by the ^{7}Li^{3+} projectile. Total charge of 1425 μC was collected over 6.25 hours' duration. Excitation functions of the evaporation residues, ^{93,94,95,96}Tc, ^{93}Mo^{m}, and ^{90,96}Nb, were measured in the projectile energy range 37–45 MeV.

2. ^{9}Be + ^{nat}Y

A pure (99.9%) yttrium foil was procured from Alfa Aesar. Thin self-supporting yttrium foils of thickness 3–3.8 mg/cm^2 were prepared by proper rolling. The target stack was assembled by placing aluminum catcher foils of thickness 1.5 mg/cm^2 between two Y foils. The target assembly was bombarded by a ^{9}Be^{4+} beam and a total 304 μC charge was collected over 3.75 hours' duration. Excitation functions of ^{93,94,95}Tc and ^{93}Mo^{m} were measured in the 30–48 MeV incident energy range.

B. Measurement of activity

The aim of this article is to study the production of ^{93,94,95,96}Tc radionuclides and the associated radionuclidic impurities produced from both reactions. The duration of the irradiation time was chosen according to the beam intensity and half-lives of the product nuclides. The targets and aluminum foils were mounted on an aluminum ring of 10 mm inner and 22 mm outer diameter with 0.5 mm thickness. The residual products, if any, recoiled in the beam direction, were completely stopped in the aluminum backing. The large area of the catcher foils ensured the complete collection of recoiled evaporation residues. At the end of the bombardment, foils were counted for the γ-ray activity of the evaporation residues by an high purity germanium (HPGe) detector of 2.13 keV resolution at 1332 keV coupled with a PC-based multichannel analyzer (MCA), second generation personal computer analyzer (PCA-2), Oxford. Efficiency calibration of the detector was performed as a function of γ-ray energy using a standard ^{152}Eu ($T_{1/2}$ = 13.506 years) source of known activity. Each foil was counted for 300 s in the live-time mode, leaving proper cooling time after the bombardment. Successive measurements were carried out for a sufficiently long time in the same geometry. In general, projectile energy at a target is the average of the incident and outgoing beam energies. Beam-energy degradation in the target and the catcher foils was calculated using Stopping and Range of Ions in Matter [25]. Energy loss was less than 2% in the case of zirconium targets, whereas it was about 4%–5% for yttrium targets. Total charge of each irradiation experiment was measured by an electron-suppressed Faraday cup stationed at the rear of the target assembly, which in turn was the measure of beam intensity. Evaporation residues recoiled to the catcher foils were also measured by γ-ray counting. It was noticed that a minute amount of radionuclides recoiled to the catcher foil only at the higher incident energies and therefore were neglected in the present calculation.

The nuclear spectroscopic data used to calculate the product yield of the evaporation residues are listed in Table I [26]. The background-subtracted peak-area count corresponding to a particular γ-ray energy is the measure of yield. The product yield (y_i) of a particular radionuclide (evaporation residue) i at the end of bombardment was calculated from the standard relation

$$y^i = \frac{c(t)}{\epsilon^i_\gamma I^i_\gamma} e^{\lambda^i \tau}, \tag{1}$$

where $c(t)$ is the count rate at any time t and ϵ^i_γ and I^i_γ are the detection efficiency and branching intensity of the characteristic γ ray of the evaporation residue, respectively. The decay constant is λ^i and cooling time is τ. The cross section of the ith evaporation residue, $\sigma^i(E)$, at an incident energy, E, is calculated from the activation equation

$$y^i = I_p \sigma^i(E) n_{tg} x_{tg} (1 - e^{-\lambda_i T}), \tag{2}$$

where I_p is the intensity of the projectile; n_{tg} and x_{tg} are the number of target nuclei per unit volume and target thickness, respectively; and T is the duration of irradiation.

TABLE I. Nuclear spectrometric data of the radionuclides produced through ^{7}Li + ^{nat}Zr and ^{9}Be + ^{nat}Y reactions. The bold γ rays were used in determining the excitation functions.

Product nuclei	Spin	$T_{1/2}$	Decay mode (%)	E_γ (keV) [I_γ (%)]
^{93}Tc	$9/2^+$	2.75 hours	ϵ(100)	**1363.09** (66), 1520.3 (23.9)
^{94}Tc^m	2^+	52.0 min	ϵ(100), IT(<0.1)	871.097 (94.2)
^{94}Tc	7^+	293 min	ϵ(100)	**702.63** (99.6), 871.097 (99.9)
^{95}Tc	$9/2^+$	20.0 hours	ϵ(100)	**765.789** (94.0), 1073.713 (3.75)
^{96}Tc^m	4^+	51.5 min	IT (98), ϵ(2)	778.196 (1.9), 1200.165 (1.09)
^{96}Tc	7^+	4.28 days	ϵ(100)	778.196 (99.76), **812.54** (82)
^{93}Mo^m	$21/2^+$	6.87 hours	IT(99.88), ϵ(0.12)	263.143 (56.7), **684.753** (99.7)
^{96}Nb	6^+	23.35 hours	β^- (100)	**568.86** (56.8), 778.196 (96.88)
^{90}Nb	8^+	14.6 hours	ϵ(100)	141.174 (66.7), **1129.195** (92.7)

C. Uncertainties in the measurements

The errors associated with the cross-sectional measurements are as follows:

(i) Error in efficiency calibration of HPGe detector is ≈2%.
(ii) Error in determining target thickness ($n_{tg}x_{tg}$) in atoms per centimeter squared is ≈5%.
(iii) Systematic error in the beam current that propagated to the cross-sectional data is ≈10–12%.
(iv) Uncertainty in the incident beam energy at the successive targets may occur because of the energy degradation in the aluminum catchers. According to Refs. [27,28], the energy straggling is expected to be small, even in case of lowest incident energy, and hence was neglected in the present work.

Apart from the preceding, error occurs in the cross-sectional data because of counting statistics. The total associated error related to the cross-sectional measurement was determined considering all the factors discussed and the data presented up to a 95% confidence level.

III. DATA ANALYSIS USING NUCLEAR REACTION MODELS

A. PACE-II

In PACE-II, the deexcitation process of the excited nuclei has been calculated using the modified version of the code JULIAN, which follows the correct procedure of angular momentum coupling at each stage of the deexcitation using the Hauser-Feshbach [29] model. The transmission coefficients for light-particle emission, such as neutrons, protons, and αs, have been determined from the optical model potential, where all the optical model parameters are taken from Ref. [30]. The shift in Coulomb barrier during deexcitation is accounted for by calculating the transmission coefficients at an effective energy determined by the shift. The code internally decides level densities and masses it needs during deexcitation. Because of low excitation energy, the Gilbert-Cameron level-density prescription is used in the present work with a, the level density parameter, equal to $A/12$ MeV^{-1}. The ratio of a_f/a_n is chosen as unity. Fission is considered as a decay mode. The finite range fission barrier of Sierk [31] has been used. The compound nuclear fusion cross section is determined using the Bass method [32]. The yrast parameter is taken as unity. A nonstatistical yrast cascade γ-decay chain has been artificially incorporated to simulate γ multiplicity and energy results.

B. ALICE91

A geometry-dependent hybrid model [24,33–35] has been used to calculate PEQ emissions and the Weisskopf-Ewing formalism [36] for EQ emissions. The hybrid model assumes that the target-projectile composite system proceeds through a two-body interaction process. Each stage of the relaxation process is designated by the total number (n) of excited particles, that is, the sum of excited particles (p) and holes (h). In each two-body interaction, p-h pairs may be created or annihilated or redistribution of energy may take place without changing the number. The hybrid model uses "never come back" approximation; that is, the model assumes only one p-h pair is created in each interaction. The hybrid model explicitly determines the preemission energy distribution of the excited particles, which helps to estimate the high-energy emissions more accurately. The geometry-dependent hybrid model includes the nuclear surface effects [24,34,35]. The PEQ emission cross section for a particular ejectile x with energy ϵ_x is given by

$$\sigma_{\mathrm{PEQ}}(\epsilon_x) = \frac{\lambda^2}{4\pi}\sum_{l=0}^{\infty}(2l+1)T_l \sum_{\substack{n=n_0,\\ \Delta n=2}}^{\overline{n}} D_n \left[f_n^x \frac{N_n(l,U,\epsilon_x)}{N_n(l,E_c)} \right] \times \frac{\lambda_c(\epsilon_x)}{\lambda_c(\epsilon_x)+\lambda_t(\epsilon_x)}, \quad (3)$$

where λ is the de Broglie wavelength of the projectile; T_l is the transmission coefficient of the lth partial wave; D_n is the depletion factor of the nth exciton state, that is, the probability of reaching the n exciton state without prior emission; and f_n^x is number of x-type excited nucleons present in it. The numbers n_0 and $\overline{n}$ are the initial and equilibrium exciton numbers, respectively. The ratio $N_n(l,U,\epsilon_x)/N_n(l,E_c)$ is the probability of finding an x-type nucleon in the n exciton state with energy $(\epsilon_x + B_x)$, where B_x is the separation energy of x. The factor $[\lambda_c(\epsilon_x)]/[\lambda_c(\epsilon_x)+\lambda_t(\epsilon_x)]$ is the emission probability of x with energy ϵ_x; $\lambda_t(\epsilon_x)$ is the two-body interaction rate. The emission

rate $\lambda_c(\epsilon_x)$ is calculated by [24]

$$\lambda_c(\epsilon_x) = \frac{(2S_x + 1)\mu_x \epsilon_x \sigma_{\rm inv}(\epsilon_x)}{\pi^2 \hbar^3 g}, \quad (4)$$

where S_x is the intrinsic spin of x, μ_x is the reduced mass, $\sigma_{\rm inv}$ is the inverse cross section of the ejectile x with energy ϵ_x being absorbed by the residual, and g is the single-particle-level density of the composite nucleus. The EQ emission cross section has been calculated using the Weisskopf-Ewing formalism as

$$\sigma_{\rm EQ}(\epsilon_x) \sim \sigma_{\rm comp} \frac{e^{2(aU)^{1/2}}}{U}, \quad (5)$$

where $\sigma_{\rm comp}$ is the compound nuclear formation cross section, a is the level-density parameter, and U is the available excitation energy of the compound nucleus after the PEQ emissions. Variable $\sigma_{\rm comp}$ has been calculated as $\sigma_{\rm comp} = \sigma_{\rm abs} - \sigma_{\rm PEQ}$, where $\sigma_{\rm abs}$ is the absorption cross section of the projectile in the target and $\sigma_{\rm PEQ}$ is the total PEQ emission cross section.

In the ALICE91 calculation, n, p, d, and α emissions are considered from residual nuclides 12 mass units wide and 10 charge units deep, including the composite nucleus. Fermi gas-level density has been used for the calculation of reaction cross sections. Reverse-channel-reaction cross sections have been calculated using the optical model. The level-density parameter a is taken as $A/12$ MeV^{-1}. The rotating finite-range fission barriers of Sierk have been chosen. The total number of nucleons in the projectile has been chosen as the initial exciton number for the PEQ cross section calculation.

IV. RESULTS AND DISCUSSION

The residual radionuclides produced through various reaction channels of ^{7}Li + $^{\rm nat}$Zr and ^{9}Be + $^{\rm nat}$Y reactions at the maximum incident energies of 44.6 MeV and 47.5 MeV, respectively, are shown in Figs. 1 and 2 with their characteristic γ rays. Experimental excitation functions of the residues are compared with the theoretical predictions of PACE-II and ALICE91 in Figs. 3–6. Experimental cross sections are represented by various symbols, with the associated error and theoretical predictions shown by the lines (solid line for PACE-II and dashed line for ALICE91). Though the code ALICE91 takes care of the PEQ emissions, it has been observed that the PEQ reaction has almost no contribution, except about 5% in the highest incident energy, in producing the evaporation residues in the energy range studied.

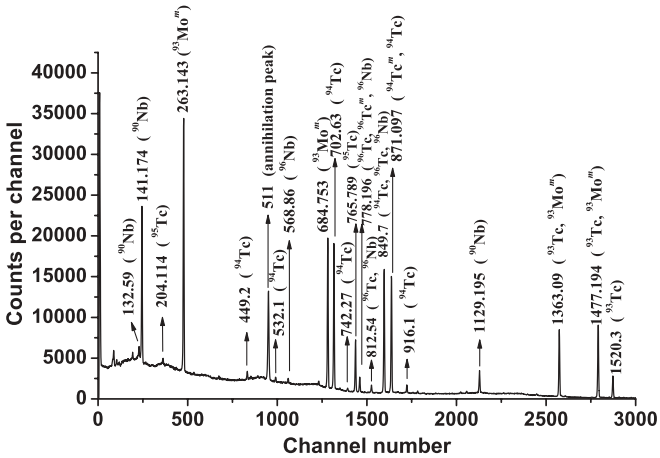

FIG. 1. The γ-ray spectrum of the radionuclides produced in ^{7}Li + $^{\rm nat}$Zr reaction at 44.6 MeV incident energy.

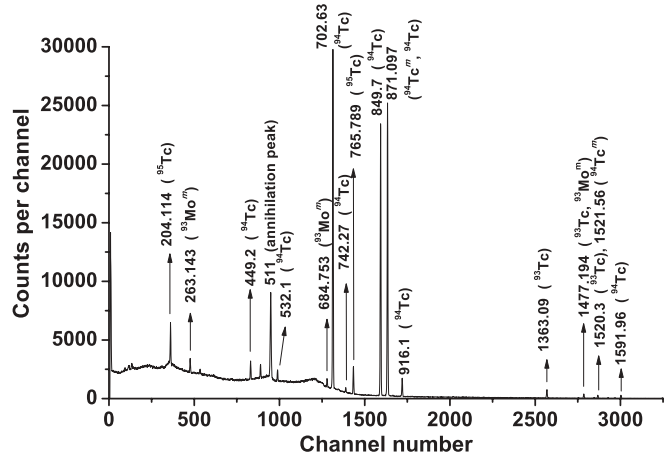

FIG. 2. The γ-ray spectrum of the radionuclides produced in ^{9}Be + $^{\rm nat}$Y reaction at 47.5 MeV incident energy.

A. ^{7}Li + $^{\rm nat}$Zr

Figure 1 shows that the Tc radionuclides, ^{93,94,95,96}Tc, are produced along with ^{93}Mo^{m} and ^{90,96}Nb radionuclides because of the bombardment of the ^{7}Li ion on $^{\rm nat}$Zr at 44.6 MeV incident energy. Measured excitation functions of ^{93,94}Tc and ^{95,96}Tc are compared with the theoretical predictions in Figs. 3 and 4, respectively, in the 37–45 MeV energy range. The natural assay of zirconium contains five naturally abundant Zr isotopes: ^{90}Zr (51.45%), ^{91}Zr (11.22%), ^{92}Zr (17.15%), ^{94}Zr (17.38%), and ^{96}Zr (2.8%). The theoretical excitation

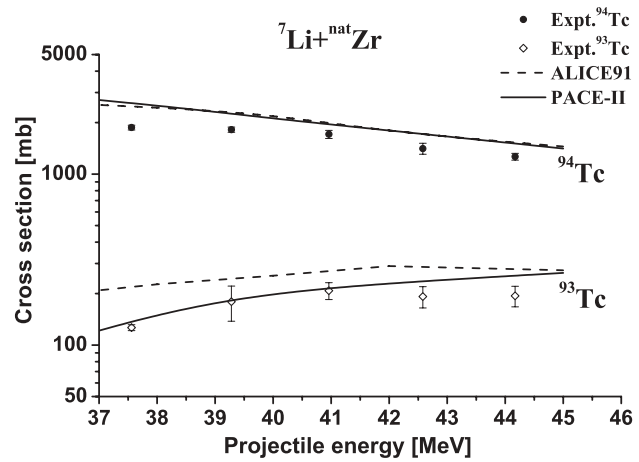

FIG. 3. Comparison between measured production cross sections of ^{93}Tc and ^{94}Tc with theoretical predictions of PACE-II and ALICE91. The cross-sectional values are multiplied by 10 for ^{94}Tc.

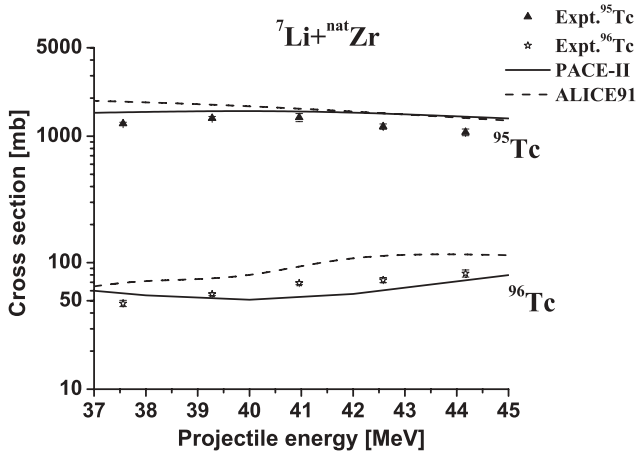

FIG. 4. Comparison between measured production cross sections of ^{95}Tc and ^{96}Tc with theoretical predictions of PACE-II and ALICE91. The cross-sectional values are multiplied by 10 for ^{95}Tc.

functions reported in Figs. 3–5 have been calculated taking the weighted average of all five natural isotopes of Zr.

It is observed from Fig. 3 that experimental cross sections of ^{93}Tc are well reproduced by the prediction of PACE-II, whereas ALICE91 overpredicts throughout the range with a maximum of 75% at 37.5 MeV incident energy. In the case of ^{94}Tc, both theoretical calculations are close to each other and slightly overpredict the experimental data. However, overall observation shows good agreement between the experimental results and PACE-II predictions.

Figure 4 shows a comparison between the measured cross sections of ^{95,96}Tc and the theoretical estimations. In both cases, experimental data agree with the PACE-II calculations. However, ALICE91 overpredicts the data throughout the range. This observation reveals that the ^{93,94,95,96}Tc radionuclides are produced as a result of complete fusion of ^{7}Li in the ^{nat}Zr target, which is according to expectations. It is observed from Figs. 3 and 4 that PACE-II calculations reproduced the measured excitation functions with a tendency toward slight

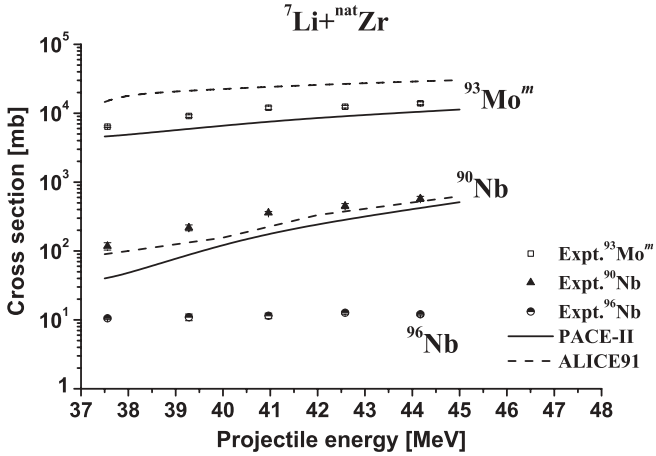

FIG. 5. Comparison between measured production cross sections of ^{93}Mo^{m} and ^{90,96}Nb with theoretical predictions. Cross-sectional values are multiplied by 100 and 10 for ^{93}Mo^{m} and ^{90}Nb, respectively.

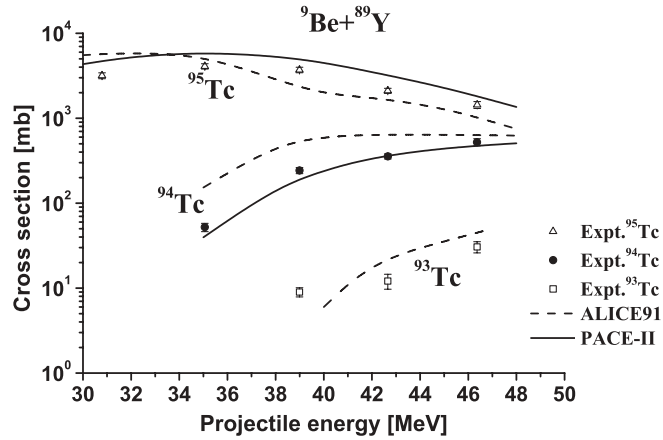

FIG. 6. Comparison between measured production cross sections of ^{95}Tc, ^{94}Tc, and ^{93}Tc with theoretical predictions of PACE-II and ALICE91. The cross-sectional values are multiplied by 10 for ^{95}Tc.

overprediction, which implies the prominent role of compound nuclear reaction mechanisms.

Figure 5 presents the experimental excitation function for the production of ^{93}Mo^{m} and ^{90,96}Nb through ^{7}Li + ^{nat}Zr reactions along with the theoretical values. The PACE-II code underpredicts the measured excitation functions of ^{93}Mo^{m} and ^{90}Nb by 25% and 50%, respectively, at lowest incident energy. ALICE91 calculation unexpectedly overpredicts the experimental excitation function of ^{93}Mo^{m} by a factor of 2, whereas it agrees with the cross sections of ^{90}Nb. Underprediction of cross-sectional values by PACE-II might be an indication of the PEQ process in formation of ^{93}Mo^{m} and ^{90}Nb. However, none of the theoretical models predicts the production of ^{96}Nb when its signature is observed experimentally.

B. ^{9}Be + ^{nat}Y

Owing to the bombardment of ^{9}Be on natural yttrium (^{89}Y), mainly ^{93,94,95}Tc are produced in the 30–48 MeV incident energy range. Only a small amount of ^{93}Mo^{m} is produced at 47.5 MeV incident energy. Figure 6 shows the experimental excitation function of ^{93,94,95}Tc along with the theoretical predictions of PACE-II and ALICE91. Measured excitation functions of ^{94}Tc are well evaluated by the PACE-II code, whereas ALICE91 overpredicts the measured data. Measured cross sections of ^{95}Tc are reproduced by both codes at higher energies; however, about 30% underprediction has been seen in the measured data at 35 MeV incident energy and less. The incident energy range reported (30–48 MeV) in the present work covers maximum production of ^{95}Tc and ^{94}Tc at the lowest and highest incident energy sides. The trend of the measured excitation function exactly matches with the PACE-II predictions. The measured excitation function of ^{93}Tc is compared only with the ALICE91 values, which start at 40 MeV incident energy, and slightly overpredicts the experimental cross sections at the next two energy values. However, the cross section has been measured at 39 MeV, which is well above the threshold value of 36.5 MeV. According to PACE-II, the ^{89}Y(^{9}Be, 5n) reaction channel will open from 45 MeV. It is clear from the cross-sectional values that Tc radionuclides

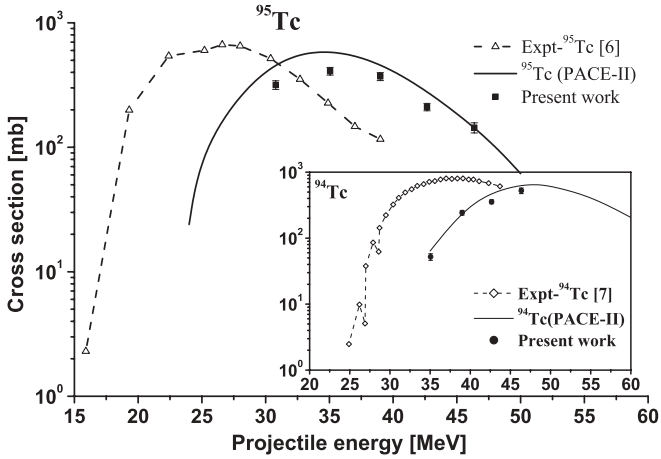

FIG. 7. Comparison between measured excitation functions of ^{95}Tc [6] and ^{94}Tc [7] from $\alpha + {}^{93}$Nb, measured excitation functions of ^{95}Tc and ^{94}Tc from the present work, and theoretical predictions of PACE-II from ^{9}Be + ^{89}Y.

are produced through ^{89}Y(^{9}Be, xn) ($n = 3, 4, 5$) reaction channels by complete nuclear fusion. This is expected when the maximum incident energy is less than 5.5 MeV/nucleon. No signature of the PEQ process has been observed from the experimental cross sections. Production of ^{93}Mo^{m} is observed only in the first foil at 47.5 MeV. The measured cross section is (13 ± 2.1) mb, which was expected from both theoretical estimations.

The basic difference in the two theoretical predictions from PACE-II and ALICE91 is observed because of the formalisms adopted for the simulation of the compound nuclear processes. ALICE91 uses the faster Weisskopf-Ewing approach, whereas PACE-II takes the Hauser-Feshbach formalism. The latter is found to be better in explaining the nuclear data obtained entirely from the compound nuclear reactions. The present work agrees with this fact. Though the PEQ contribution was observed near the reaction threshold in some heavy-ion reactions, it is not significant in these two cases.

To understand the production of ^{95}Tc and ^{94}Tc quantitatively from the light- and heavy-ion-induced reactions on mononuclidic natural targets, Fig. 7 compares the excitation functions of ^{95}Tc and ^{94}Tc from (i) the $\alpha + {}^{93}$Nb reaction [6,7], (ii) the theoretical predictions of PACE-II for the ^{9}Be + ^{89}Y reaction, and (iii) those measured from the present work. It is observed from the figure that the theoretical expectation of the production of ^{95,94}Tc from the ^{9}Be + ^{89}Y reaction is comparable to that measured from the $\alpha + {}^{93}$Nb reaction. This article is important for establishing this observation. The trends of the measured excitation functions of ^{95}Tc and ^{94}Tc are in accord with the PACE-II prediction, however, the absolute value of the measured cross section for ^{95}Tc is 30% underpredicted at 35 MeV and less projectile energies, while production cross sections of ^{94}Tc agree well with the theory in the reported projectile energy range.

V. CONCLUSION

This article reports two new production routes of the proton-rich Tc radionuclides via heavy-ion-induced reactions of ^{7}Li + ^{nat}Zr and ^{9}Be + ^{nat}Y. Excitation functions of the evaporation residues produced from these reactions have been measured in the energy ranges 37–45 MeV and 30–48 MeV, respectively. The measured cross-sectional values were found to be in good agreement with the detailed Hauser-Feshbach model calculations using the PACE-II code. The cross-sectional data essentially revealed the compound nuclear reaction mechanism as per expectations in the energy range studied. Experimental nuclear reaction data are important for the quality production of Tc radionuclides.

In the case of the ^{7}Li + ^{nat}Zr reaction, reported incident energy range 37–45 MeV is not sufficient to get a complete picture of the excitation functions of evaporation residues. More experimental data are needed at both higher and lower incident energies. However, the presence of all other radionuclides, which may cause difficulty in optimizing production parameters of a particular isotope of interest, reducing other radionuclidic impurity, is prominent from the study. The overall knowledge of the work will be helpful in producing clinically important proton-rich Tc radionuclides. The cross-sectional data will also help to increase radionuclidic purity, optimizing nuclear reaction parameters. However, it is once again clear that the mononuclidic target has an advantage in this context.

ACKNOWLEDGMENTS

The authors are thankful to the TIFR target laboratory and Pradipta Das from SINP for preparing zirconium and yttrium targets, respectively. Thanks to the staff of the TIFR Pelletron for their kind support and help during the experiments. M.M. is thankful to the Council of Scientific and Industrial Research. This work has been carried out as a part of the Saha Institute of Nuclear Physics, Department of Atomic Energy, XI 5-year plan project "Trace Analysis: Detection, Dynamics, and Speciation."

[1] C. L. Branquinho, S. M. Hoffmann, G. W. A. Newton, V. J. Robinson, H. Y. Wang, I. S. Grant, and J. A. B. Goodall, J. Inorg. Nucl. Chem. **41**, 617 (1979).
[2] N. R. Ramamoorthy, M. K. Das, B. R. Sarkar, and R. S. Mani, J. Radioanal. Nucl. Chem. **98**, 121 (1986).
[3] L. T. Auler, A. G. Da Silva, and G. W. A. Newton, J. Inorg. Nucl. Chem. **43**, 2611 (1981).
[4] M. Fassbender, A. F. Novgorodov, F. Roesch, and S. M. Qaim, Radiochim. Acta **65**, 215 (1994).
[5] B. Strohmaier, M. Fassbender, and S. M. Qaim, Phys. Rev. C **56**, 2654 (1997).
[6] M. K. Sharma, H. D. Bhardwaj Unnati, P. P. Singh, B. P. Singh, and R. Prasad, Eur. Phys. J. A **31**, 43 (2007).
[7] F. Tarkanyi, F. Ditroi, F. Szelecsenyi, M. Sonck, and A. Hermanne, Nucl. Instrum. Methods B **198**, 11 (2002).
[8] E. A. Shakun, V. S. Batii, Y. N. Rakivnenko, and O. A. Rastrepin, Sov. J. Nucl. Phys. **46**, 17 (1987).

[9] M. C. LagunasSolar and R. P. Haff, Radiochim. Acta **60**, 57 (1993).
[10] F. Rosch and S. M. Qaim, Radiochim. Acta **62**, 115 (1993).
[11] M. S. Uddin and M. Baba, Appl. Radiat. Isot. **66**, 208 (2008).
[12] M. S. Uddin, M. Hagiwara, F. Tarkanyi, F. Ditroi, and M. Baba, Appl. Radiat. Isot. **60**, 911 (2004).
[13] M. U. Khandaker, K. Kim, Y. S. Lee, and G. Kim, J. Kor. Phys. Soc. **50**, 1518 (2007).
[14] Z. Randa and K. Svoboda, J. Inorg. Nucl. Chem. **38**, 2289 (1976).
[15] M. Bonardia, C. Birattaria, F. Groppia, and E. Sabbionib, Appl. Radiat. Isot. **57**, 617 (2002).
[16] J. Luo, F. Tuo, X. Kong, R. Liu, and L. Jiang, Appl. Radiat. Isot. **66**, 1920 (2008).
[17] J. Luo, G. Liu, F. Tuo, X. Kong, R. Liu, L. Jiang, and B. Lou, Phys. Rev. C **76**, 057601 (2007).
[18] T. Sekine, K. Yoshihara, J. Safar, L. Lakosi, and A. Vertes, J. Radiol. Nucl. Chem. **186**, 165 (1994).
[19] P. Misaelides, Radiochim. Acta **28**, 1 (1981).
[20] B. B. Kumar, S. Mukherjee, S. Chakrabarty, B. S. Tomar, A. Goswami, and S. B. Manohar, Phys. Rev. C **57**, 743 (1998).
[21] M. Maiti and S. Lahiri, Phys. Rev. C **79**, 024611 (2009).
[22] A. Gavron, Phys. Rev. C **21**, 230 (1980).
[23] M. Blann, Lawrence Livermore National Laboratory Report No. UCID 19614, 1982 (unpublished); M. Blann, paper SMR/284-1 in Proceedings of the International Centre for Theoretical Physics Workshop on Applied Nuclear Theory and Nuclear Model Calculations for Nuclear Technology Applications, Trieste, Italy, 1988 (unpublished).
[24] M. Blann and H. K. Vonach, Phys. Rev. C **28**, 1475 (1983).
[25] J. F. Ziegler, J. P. Biersack, and U. Littmark, *The Stopping and Range of Ions in Solids* (Pergamon, New York, 1985).
[26] R. B. Firestone and V. S. Shirley, *Table of Isotopes*, 8th ed. (Wiley, New York, 1996).
[27] B. Wilke and T. A. Fritz, Nucl. Instrum. Methods **138**, 331 (1976).
[28] J. Kemmer and R. Hofmann, Nucl. Instrum. Methods **176**, 543 (1980).
[29] W. Hauser and H. Feshbach, Phys. Rev. **87**, 366 (1952).
[30] C. M. Perey and F. G. Perey, At. Data Nucl. Data Tables **17**, 1 (1976).
[31] A. J. Sierk, Phys. Rev. C **33**, 2039 (1986).
[32] R. Bass, Phys. Rev. Lett. **39**, 265 (1977).
[33] M. Blann, Phys. Rev. Lett. **27**, 337 (1971); **27**, 700(E) (1971); **27**, 1550(E) (1971).
[34] M. Blann, Nucl. Phys. **A213**, 570 (1973).
[35] M. Blann, Phys. Rev. Lett. **28**, 757 (1972).
[36] V. F. Weisskopf and D. H. Ewing, Phys. Rev. **57**, 472 (1940).